

Characterization of semiconductor materials and devices using acoustoelectric voltage measurement

M. TabibAzar, M. N. Abedin, Agostino Abbate, and P. Das

Citation: *Journal of Vacuum Science & Technology B* **9**, 95 (1991); doi: 10.1116/1.585796

View online: <http://dx.doi.org/10.1116/1.585796>

View Table of Contents: <http://scitation.aip.org/content/avs/journal/jvstb/9/1?ver=pdfcov>

Published by the AVS: Science & Technology of Materials, Interfaces, and Processing

Articles you may be interested in

[Acoustoelectric coupling for direct electrical characterization of semiconductor devices](#)

J. Appl. Phys. **99**, 063712 (2006); 10.1063/1.2186025

[Challenges for materials and device characterization in the semiconductor industry](#)

AIP Conf. Proc. **388**, 133 (1997); 10.1063/1.52172

[Characterization of ZnSe/GaAs heterostructure using transverse acoustoelectric voltage spectroscopy](#)


Appl. Phys. Lett. **60**, 862 (1992); 10.1063/1.107433

[Calculation of the transverse acoustoelectric voltage in a piezoelectricextrinsic semiconductor structure](#)

J. Appl. Phys. **66**, 1209 (1989); 10.1063/1.343465


[Semiconductor surface characterization using transverse acoustoelectric voltage versus voltage measurements](#)

J. Appl. Phys. **54**, 415 (1983); 10.1063/1.331721




Instruments for Advanced Science

Contact Hiden Analytical for further details:
W www.HidenAnalytical.com
E info@hiden.co.uk
[CLICK TO VIEW](#) our product catalogue




Gas Analysis

- » dynamic measurement of reaction gas streams
- » catalysis and thermal analysis
- » molecular beam studies
- » dissolved species probes
- » fermentation, environmental and ecological studies




Surface Science

- » UHV TPD
- » SIMS
- » end point detection in ion beam etch
- » elemental imaging - surface mapping



Plasma Diagnostics

- » plasma source characterization
- » etch and deposition process reaction
- » kinetic studies
- » analysis of neutral and radical species



Vacuum Analysis

- » partial pressure measurement and control of process gases
- » reactive sputter process control
- » vacuum diagnostics
- » vacuum coating process monitoring

Characterization of semiconductor materials and devices using acoustoelectric voltage measurement

M. Tabib-Azar

Electrical Engineering and Applied Physics Department, Case Western Reserve University, Cleveland, Ohio 44106

M. N. Abedin

NASA Langley Research Center, Nondestructive Measurement Science Branch, Hampton, Virginia 23665

Agostino Abbate and P. Das

Electrical, Computer, and Systems Engineering Department, Rensselaer Polytechnic Institute, Troy, New York 12180-3950

(Received 19 February 1990; accepted 1 October 1990)

During the past 20–25 years, the nondestructive surface acoustic wave (SAW) measurement technique has been developed and used to characterize the electrical properties of semiconductor materials and devices. Important semiconductor parameters such as carrier density, type and mobility, interface and fixed oxide charge densities, deep-level cross section and activation energy, and excess carrier generation and recombination lifetimes are all determined using SAW. In the majority of these experiments, separate medium structure is used where SAW is generated at the surface of a piezoelectric substrate like LiNbO_3 . SAW in the piezoelectric materials is accompanied by a decaying electric field which interacts with the free carriers of a semiconductor placed nearby. The spatial resolution that is usually achieved in these measurements is on the order of the SAW wavelength or the extrinsic Debye length, whichever is shorter. Variety of semiconductors are characterized using SAW including: silicon, GaAs, $\text{Al}_x\text{Ga}_{1-x}\text{As}$, InAs, GaP, $\text{Hg}_x\text{Cd}_{1-x}\text{Te}$, CdTe, InP, CdS, and InAs. More recently, high T_c ceramic superconductors have also been studied. The most important aspect of the SAW technique is that it is nondestructive and it has very high sensitivity in studying high resistivity materials. Here, we present a review of the SAW technique discussing its application in quantitative characterization of semiconductor materials and devices.

I. INTRODUCTION

Interaction of an electron system with a phonon system has always been of interest in solid-state physics. Whether the interaction between these two systems comes about through the piezoelectric effect, it offers some interesting prospect in control/modification or study of the properties of one of these systems by the other one. In this respect, acoustoelectric interaction in superconductors,¹ acoustic wave amplifiers² and their more promising successors, surface acoustic wave amplifiers,^{3–6} and acoustic charge transport devices,⁷ and phonon transmission spectroscopy of $\text{Al}_x\text{Ga}_{1-x}\text{As}$ /GaAs superlattice⁸ are among the important examples.

Acoustoelectric interaction (AEI) was first discussed by Weinrich where he showed that ultrasound propagating in a metal is attenuated due to the interaction with the free electrons. A dc acoustoelectric voltage was predicted to be developed due to the transfer of energy from ultrasound to free electrons. The coupling of the ultrasound and free electrons in metals was due to the deformation potential. Later, the work was extended to piezoelectric semiconductors where the effect was more dramatic due to the piezoelectric coupling.^{2,9–12} Cadmium sulphide, gallium arsenide and other semiconductors were used in conjunction with bulk compressional and shear waves to study ultrasonic attenuation and change in the wave velocity due to the acoustoelectric interaction.^{10,11}

These studies were extended to amplification of ultra-

sound when a dc electric bias field was superimposed.¹⁰ As the bias field moves the free carriers faster than the velocity of ultrasound, through the piezoelectric coupling the free carriers transfer energy to the ultrasound giving rise to its amplification.¹¹ Later, AEI was extended to surface acoustic wave (SAW) devices.^{3–6,13–19} For SAW devices, there are two possible structures. These are so called combined medium and separate medium structures. In the combined medium structure, surface waves propagate on a piezoelectric semiconductor like GaAs and CdS. The elastic wave generates the electric field which interacts with the free carriers giving rise to a acoustoelectric interaction. However, in a separate medium structure, the surface wave is generated on a piezoelectric insulator such as LiNbO_3 . A semiconductor, which need not be piezoelectric (e.g., silicon), is placed near the piezoelectric substrate where SAW is generated.¹¹ Thus the electric field of the SAW interacts with the free carriers of the semiconductor. The separate medium structure is ideal for ultrasonic amplification because one can optimize the parameters of the piezoelectric substrate where SAW is generated.¹¹ Thus the electric field of the SAW interacts with the free carriers of the semiconductor. The separate medium structure is ideal for ultrasonic amplification because one can optimize the parameters of the piezoelectric substrate and free the carriers of semiconductors.³

Surface acoustic waves (Rayleigh waves) also offered an additional attraction by having larger energy density²⁰ compared to the bulk waves. Also, transducers could be made

right at the surface using thin metallic films and photolithography and, most importantly, separate medium configuration could be realized by interacting acoustic waves in a piezoelectric medium with free carriers in an adjacent semiconductor medium.²⁰

The separate medium configuration is shown in Fig. 1. Using planar transducers, a radio frequency (rf) pulse is converted to a surface acoustic wave (SAW) in the piezoelectric medium. Y-cut, z-propagating LiNbO_3 , due to its relatively large piezoelectricity, is usually used. The electric field that accompanies the SAW in the LiNbO_3 decays exponentially above the surface.^{3,13-19} The interaction of this field with the free carriers of the semiconductor that is placed at the surface of the LiNbO_3 is called the acoustoelectric interaction (AEI). AEI results in the following interesting acoustoelectric signals in the semiconductor: (i) a dc voltage/current across the semiconductor in the direction perpendicular to the surface,^{13,14,17} (ii) a dc voltage/current along the semiconductor in the direction parallel to the surface,^{15,21} and (iii) similar ac signals at twice the frequency of the SAW.²² The above signals are called acoustoelectric voltages or currents (AEV or AEC). AEI also modifies the SAW parameters. SAW is attenuated and its velocity is changed.^{3,14,15}

There is also a possibility of sending two contradirected SAW that result in convolution signals in the semiconductor. This effect has been extensively studied in the context of nonlinear signal-processing devices.^{22,23}

Using the above effects variety of device ideas were conceived and constructed.²⁷ These include: acoustic wave delay lines (due to five orders of magnitude difference between the SAW velocity and speed of light, millisecond delays can be conveniently achieved), acoustic wave amplifiers,³ acoustic charge transport devices,⁷ convolvers, correlators, matched filters, imaging devices²⁵ (basically using SAW as a scanner), and acousto-optic signal processing devices and scanners.^{22,24-26}

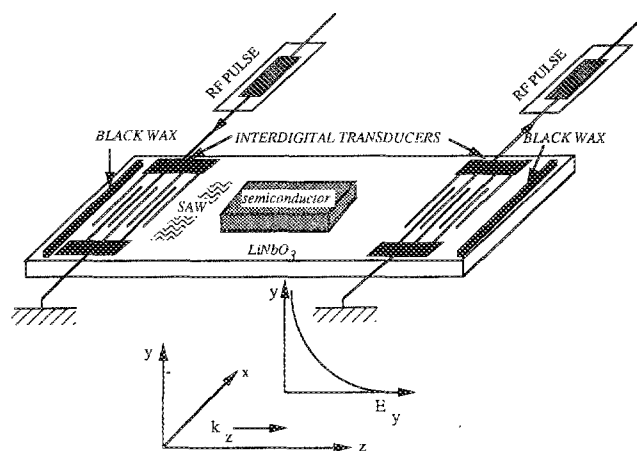


FIG. 1. Separate medium configuration SAW is generated at the surface of a piezoelectric substrate (LiNbO_3). The semiconductor is simply placed on top of the piezoelectric substrate. The acoustoelectric interaction takes place between the electric field of the SAW and the free carriers of the semiconductor. The coupling between the electric field and the free carriers is through the air.

As far as the characterization of the electrical properties of semiconductors were concerned, separate medium structure offered an alternative^{14,21,27-72} to other more conventional methods that were not nondestructive. By simply placing a semiconductor at the surface of a LiNbO_3 delay line where SAW is propagating, acoustoelectric voltages could be detected that are functions of carrier density and mobility.^{14-19,29,30,35} In the past 20 years that this idea has been pursued, drastic improvements in applying external excitations to the semiconductor has been achieved. Especially during the past eight years, two-beam spectroscopy^{34,39,41,42,63,66,73} and field-effect measurements^{40,43,47-50-53,68} have been incorporated with the basic SAW technique to obtain the energy of impurity levels^{32,39,42,44,47,49,57,64,73} and the energy profiles of interface trap densities in the band gap.^{42,49,63} Using AEV as a function of temperature measurements, deep level spectroscopy has been performed^{67,69} and a carrier profiling method similar to the profiling by capacitance versus voltage method is developed.^{40,43}

Variety of materials are characterized among which Si and GaAs are studied more extensively,^{27-30,32,39-43,48,49,51,53-55,61-63,66,69,71,73} $\text{Hg}_{1-x}\text{Cd}_x\text{Te}$ has been the most difficult one to study,^{47,50,62} and $\text{Al}_x\text{Ga}_{1-x}\text{As}/\text{GaAs}$ superlattice have yielded the most interesting and puzzling results.^{54,55,66,72,73} There are also some interesting studies showing anomalous AEV in the plane of SAW but perpendicular to the SAW direction,⁵² and numbers of different reports on the SAW-superlattice interaction.^{56,59,65}

More recently, high T_c ceramic superconductors have been nondestructively studied using the SAW technique.^{70,71} It is well known that stable electrical contacts are extremely difficult to make to ceramic superconductors and the SAW technique eliminates this need and it also gives information about the carrier type as well as determining T_c . Moreover, the SAW technique does not have complexities associated with the interpretation of the ac susceptibility measurements.

On the device side, a silicon diode array has been studied⁵⁸ and some work was performed to study $\text{Hg}_{1-x}\text{Cd}_x\text{Te}$ diode arrays as well. Leakage current in these arrays, which is the most important measure of their quality, has been measured successfully.

On the theoretical side, basic studies of acoustoelectric interaction have been reviewed recently in³⁵ and some attempts have been made to resolve some of the past contradicting results.^{35,68,74} Also, some attempts have been made to study AEI in nonflat band and layered semiconductors.^{38,56,59,65} These have yielded interesting predictions and results. However, experimental results are far richer than their theoretical explanations in nonhomogeneous systems and more theoretical studies are needed in that area.

Despite all these achievements, the SAW technique is mainly a research tool still waiting to be adopted by the industry. This is mainly due to the highly controlled conditions in which the measurements have to be performed. From a commercial point of view this makes the measurement procedure complex and laborious. On the other hand,

as a research tool it has proved its usefulness, by means of its adaptability for various different materials and measurement conditions. It is our goal in this review to discuss all the advantages and disadvantages of the SAW technique. In Secs. II and III the basic operation principles and some theoretical background of the SAW method are described, while the various characterization techniques are reviewed in the successive sections.

II. SURFACE ACOUSTIC WAVE TECHNIQUE: BASIC PRINCIPLES

As we have already mentioned in the introduction, the central feature of this technique is a delay line which consists of a piezoelectric substrate with a highly polished surface on which interdigital transducers (IDTs) are formed using photolithographic techniques. The piezoelectric material is usually a y-cut, z-propagating LiNbO₃ substrate. The IDTs are thin film aluminum fingers alternately connected to bus pads as shown in Fig. 2(a). The SAW, generated by applying rf pulses to IDTs, propagates along the surface of the substrate creating stress variations which decay exponentially with depth into the substrate. Because of the piezoelectric effect, the propagating stress waves are coupled to propagating electric fields which have component both perpendicular and parallel to the surface of LiNbO₃.

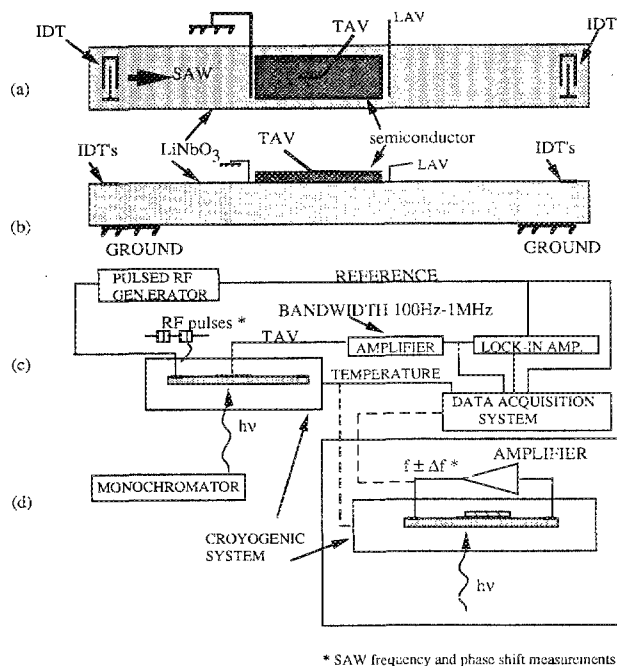


FIG. 2. The experimental set-up to study semiconductors using the SAW technique. The semiconductor is placed over the SAW delay line. The transverse acoustoelectric voltage (TAV) and the longitudinal acoustoelectric voltage (LAV) are measured across and along the semiconductor as shown in (a) and (b), respectively. The experimental set-up is shown in (c). The instruments are used as follows: Lock-in amplifier to detect the ae signals, the data-acquisition system to acquire and to analyze the data, and the monochromator for spectroscopy, a cryogenic system for low temperature measurements, and the arrangement of the delay line in the feedback of an rf amplifier in the SAW frequency and phase measurements.

The electric field exists inside and outside the piezoelectric substrate and it decays exponentially with distance from the surface.²⁰ The decay constant in the free space above the delay line is the reciprocal of the SAW wave number ($1/k$, where $k = 2\pi/\lambda$).³⁰ This electric field interacts with the free carriers of the semiconductor which is placed at the surface of the delay line [Fig. 2(b)]. Because of this interaction, some amount of energy is absorbed from the surface wave and acoustoelectric signals are developed inside the semiconductor. The semiconductor sample that is placed at the surface of the LiNbO₃ delay line is slightly pressed against the LiNbO₃ using a mechanical probe. This mechanical probe is also used as an electrode to capacitively detect any voltages that develop across the semiconductor due to the acoustoelectric interaction (AEI).

Acoustoelectric signals can be detected in two different ways [Fig. 2(a)]: (i) across the semiconductor in the direction perpendicular to the SAW propagation plane; the transverse acoustoelectric voltage (TAV),¹³⁻¹⁷ (ii) along the semiconductor in the direction parallel to the SAW propagation plane; the longitudinal acoustoelectric voltage (LAV).^{15,21} The polarities and magnitudes of these signals depend on the type of the semiconductor free carriers, their concentration, and mobility, the permittivity of the semiconductor, and the SAW parameters.^{21,30,33,35} These are discussed in the next section. Other effects of the acoustoelectric interaction include: change in the SAW velocity, the attenuation of the output signal (propagation losses),^{14,15} and the generation of convolution voltages (at 2ω , where ω is the SAW frequency) across the semiconductor.²² Convolution voltages are used in the characterization of diode arrays.⁵⁸

As will be discussed in the next section, the TAV is a function of the surface conductivity and its polarity is determined by the carrier type, being negative in *p*-type materials and positive in *n*-type materials. The TAV waveform that develops in response to the SAW pulse across a Si sample is shown in Fig. 3. To be able to detect the TAV signal capacitively, the 55 MHz rf signal is pulsed. The TAV is negative and its amplitude is 1 mV (amplification of 500). The polarity of the TAV being negative indicates that the Si sample is *p*-type. The rise and fall time of TAV, τ_1 and τ_2 , are 0.12, and 0.5 ms, respectively. These transients are related to the car-

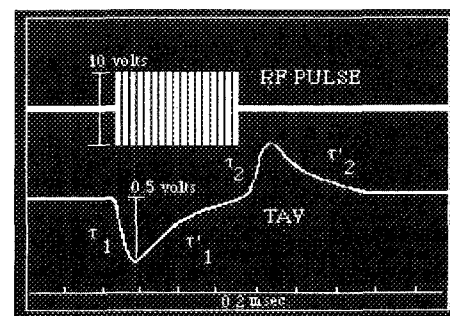


FIG. 3. The SAW rf pulse and the resulting TAV detected across a *p*-type silicon.

rier recombination/generation rate,^{28,32,51,67,72} and as will be discussed in Secs. VI and VIII, they are used in deep level studies and carrier lifetime measurements.

There are variety of external parameters that can be used as an excitation to obtain information about the opto-electrical characteristics of semiconductors. The most important of these external excitations include: temperature (T), SAW power (P_{SAW}) and frequency (ω_{SAW}), absorbed SAW power (P_{abs}), incident photon energy (E_{ph}), and dc bias voltage (V_b). Semiconductors are characterized by monitoring the acoustoelectric signals as a function of these external excitations. Surface generation velocities, fixed oxide charge density, and flat band voltage are obtained by comparing experimental and theoretical TAV- V_b curves. TAV- E_{ph} and TAV- T measurements are used to detect impurity and deep levels inside the bandgap. The carrier mobilities are obtained from LAV- P_{abs} and TAV- P_{abs} measurements.

The instrumentation to monitor the acoustoelectric signals is relatively simple [Fig. 2(c)]. Usually a high input impedance amplifier with an adjustable band pass filter is used in the case of the TAV and LAV measurements. Depending on the SAW power level and frequency, semiconductor resistivity, and the size of the air gap between the semiconductor and the delay line, typical TAV and LAV signals are between tenth of a millivolt and a fraction of a volt. Therefore, amplification of a few hundred to a few thousand is used. The output of the amplifier is usually connected to a lock-in amplifier which provides a dc voltage proportional to the acoustoelectric voltage amplitude. The output of the lock-in amplifier is either recorded using an analog x-y recorder or it is applied to a computerized data acquisition system. In the carrier lifetime measurements where the transients of the acoustoelectric signals are of interest, the lock-in amplifier is omitted or it is used in a manner similar to deep-level transient measurements. Some of the authors have used a digitizing oscilloscope to replace the lock-in amplifier and the data acquisition system.

To perform spectroscopies, light is directed at the semiconductor surface where AEI takes place (Fig. 2) and the AEV is monitored as a function of photon energy.^{34,39,41,49,54,57,63} To perform AEV as a function of temperature measurements, the LiNbO₃ delay line box is placed at the cold-head of a cryogenic system and the AEV is monitored as a function of the temperature.^{54,55,57,63,67} The field effect measurements are performed using a modified SAW delay line^{40,43,48,49,53} and they are discussed in Sec. V. In deep level and carrier lifetime measurements, the TAV transients are measured as a function of an external dc electric field^{46,51} or temperature as discussed^{63,67,69} in Secs. VI and VIII. Other measurements such as LAV- P_{abs} ⁶² and TAV- ω_{SAW} ⁵⁵ are discussed in Secs. VIII and IX.

AEI results in changes in the SAW parameters (its velocity, amplitude and phase) and the attenuation of SAW is clearly such an effect. A change in the imaginary part of the SAW wave vector (i.e., SAW attenuation constant) will result in the real part of its wave vector, which means a change in the phase of the SAW, as discussed in the next section. This can be utilized to characterize the semiconductors by measuring the change in the phase of the SAW which can be

monitored using homodyning or by using the SAW delay line as an oscillator and monitoring its resonant frequency.¹⁴ The experimental Set-up to measure the change in the SAW resonant frequency is shown in Fig. 2(c).

In SAW measurements the mechanical loading of the SAW by the semiconductor should be avoided. This is accomplished by putting spacers, that provide an air gap, between the delay line and the semiconductor. In the TAV measurements we have observed that this air gap is not essential. In the LAV and SAW phase and velocity measurements, spacers are necessary to obtain reproducible results.

III. THEORETICAL CONSIDERATIONS

The TAV is related to the carrier concentration and mobility through the following procedure.^{14,17,30,35} The modulation in the carrier concentration [$n^{(1)}e^{J(\omega t - kz)}$, $p^{(1)}e^{J(\omega t - kz)}$], where $n^{(1)}$ denotes the electron concentration and $p^{(1)}$ denotes the hole concentration and the electric field [$E^{(1)}e^{J(\omega t - kz)}$] inside the semiconductor that results due to the passage of the SAW (with frequency ω and wave vector k) is determined using the semiconductor constitutive equations [superscript (1) denotes the first-order terms proportional to the amplitude of the excitation wave]. The coordinate system is shown in Fig. 1. A nonlinear current density (J_{nl}) is defined as follows³⁰:

$$J_{\text{nl}} = \langle \sigma^{(1)} E_y^{(1)*} \rangle, \quad (1)$$

where $\sigma^{(1)}$ is the conductivity [$\sigma^{(1)} = e[\mu_n n^{(1)} + \mu_p p^{(1)}]$, e being the electronic charge], μ_n and μ_p are, respectively, electron and hole mobilities, and the brackets denote an average over a wave period. J_{nl} is then used as a source term in the current density equation and in conjunction with the continuity equation and the Poisson relationship, an inhomogeneous differential equation for the dc electric field [$E_y^{(0)}$] inside the semiconductor is derived. The solution of this differential equation along with the appropriate boundary conditions yields the $E_y^{(0)}(y)$ from which the dc potential [$\phi^{(0)}$] inside the semiconductor is obtained by integration [superscript (0) denotes second-order terms at zero frequency, i.e., the dc acoustoelectric terms needed in the calculation of TAV].

The TAV is defined as the difference of the dc potential across the semiconductor. In bulk semiconductors and at SAW frequencies less than the dielectric relaxation frequencies (i.e., $\omega_{\text{SAW}} < \omega_{\text{Cn}}$), TAV is given by³⁰:

$$\text{TAV} = V_0 \frac{(n\mu_n - p\mu_p)}{(n\mu_n + p\mu_p)} \times \frac{1}{[\omega^2 R^2 (1 + \epsilon_p/\epsilon_s)^2 + (\gamma + \epsilon_p/\epsilon_s)^2]}, \quad (3)$$

where n, p = free electron and hole concentrations within the interaction region (cm^{-3}), μ_n, μ_p = electron and hole mobilities ($\text{cm}^2/\text{V s}$), ω = SAW angular frequency (rad/s), ϵ_p = relative permittivity of the piezoelectric substrate, ϵ_s = relative permittivity of the semiconductor under study, and

$$\gamma^2 = 1 + (\omega_{\text{Cn}}\omega_{\text{Dn}} + \omega_{\text{Cp}}\omega_{\text{Dp}})/\omega^2, \quad (4)$$

where

$$\omega_{Cn} = e\mu_n n / \epsilon_s, \quad \omega_{Cp} = e\mu_p p / \epsilon_s, \quad e = \text{electronic charge},$$

$$\omega_{Dn} = V_s^2 / D_n, \quad \omega_{Dp} = V_s^2 / D_p, \quad V_s$$

$$= \text{SAW velocity (cm/s)},$$

and

$$R = (\omega_{Cn}\omega_{Dn}^2 + \omega_{Cp}\omega_{Dp}^2) / (\omega_{Cn}\omega_{Dn} + \omega_{Cp}\omega_{Dp})^2. \quad (5)$$

The constant V_0 in Eq. (3) is related to the temperature, piezoelectric coupling efficient, frequency and the acoustic power. It should be noted that in deriving the above equations it is assumed that the dc carrier densities at the surface of the semiconductor are not significantly altered due to the nonlinear SAW-semiconductor interaction. The dielectric relaxation frequencies of electron and hole systems (ω_{Cn} and ω_{Cp}) and their diffusion frequencies (ω_{Dn} and ω_{Dp}) determine the response of these system to the oscillating electric field of the SAW. As the SAW frequency becomes larger than the dielectric relaxation frequency, the TAV undergoes a sign change. This phenomena becomes important when characterizing high-resistivity GaAs where the carrier concentration and, hence, the dielectric relaxation frequency can be altered by many orders of magnitudes by changing the temperature or by photogeneration. The diffusion frequency determines the importance of the diffusion process, compared to the drift process, in the semiconductor at any given SAW frequency and velocity. Diffusion constant is a slowly varying function of the temperature and other relevant external excitations, and the SAW velocity is almost independent of these external excitations.

In Fig. 4 the behavior of the dc excess carrier concentration [$n^{(0)}$], the dc electric field [$E^{(0)}$], the dc acoustoelectric potential [$\phi^{(0)}$] and the nonlinear acoustoelectric current density (J_{nl}) inside the semiconductor are shown. The AEI tends to accumulate the semiconductor surface and to deplete the region beneath the surface. This is an important point that apparently has been overlooked by many investigators and although it was known to us through experimental observations, it was first reported in Ref. 35. Figure 4 is obtained for a high resistivity GaAs for a 55 MHz SAW. It can be seen that within one SAW wavelength of $\sim 60 \mu\text{m}$, the dc electric field, produced by AEI, reaches its maximum. In low resistivity materials the Debye length can be consider-

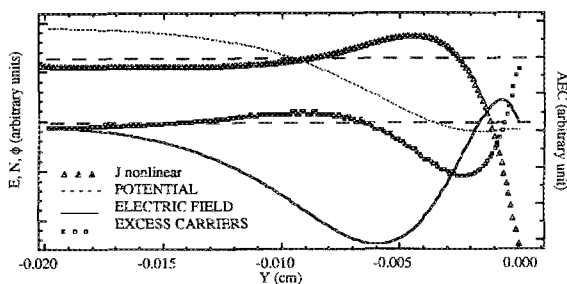


FIG. 4. The electric field (solid line), the potential (dotted line), the excess carrier concentration (squares) and the nonlinear current density (triangles) profiles inside GaAs. The semiconductor is at $y < 0$ and its surface is at $y = 0$.

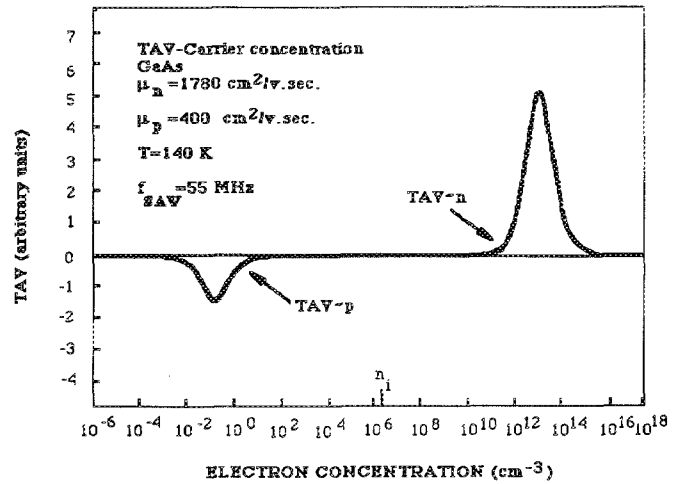


FIG. 5. The calculated TAV vs carrier concentration plot for GaAs. The curve is obtained using experimentally measured carrier mobilities.

ably shorter than the SAW wavelength and most of the variations in the carrier density and the AE field occurs within one Debye length. Therefore, the characteristic length determining the AEI is the Debye length or the SAW wavelength, whichever is shorter.

Figure 5 shows the calculated transverse acoustoelectric voltage (TAV), as a function of electron concentration (TAV-n) in GaAs.⁶³ TAV is directly proportional to the carrier concentration in a range where $10^6 \leq n < 10^{12} \text{ cm}^{-3}$ and $10^6 \leq p < 10^{12}$. Also, as mentioned before, it is negative in p -type semiconductors, and it is positive in n -type semiconductors. This property of the TAV is used to identify the type of carriers at the semiconductor surface under different conditions. The TAV-n that is shown in Fig. 5 is typically the same in other semiconductors. The relative magnitude of the positive and negative TAV peaks and its zero-crossing point is determined by the relative magnitude of the electron and hole mobilities.

The other acoustoelectric voltages and currents are derived in the above manner. In the case of the TAV the problem was solved in essentially one dimension with the z dependence of the SAW electric field only coming into play through the Laplacian and it was assumed that there is no decay of this electric field magnitude in the SAW propagation direction. In the case of the LAV, it is assumed that the SAW amplitude and its electric field decays exponentially in the z direction but the decay constant and the damping is very small so that within one wavelength it can be assumed that SAW amplitude is almost constant. This enables us to use the perturbation techniques.^{15,21,33} The energy lost through this decay gives rise to the longitudinal acoustoelectric signals. In a semiconductor where both the electron and hole conductivities are comparable, LAV is given by⁶²:

$$\text{LAV} = R_t \frac{P_{\text{abs}}}{LV_s} \left(\frac{\mu_n n - \mu_p p}{n + p} \right), \quad (6)$$

where R_t is the terminal resistance (measured directly or calculated from the geometry and the resistivity), V_s is the SAW velocity, P_{abs} is the absorbed SAW power, L is the

distance between the two LAV probes (shown in Fig. 2), n and p are the electron and hole concentrations respectively, and μ 's are the corresponding mobilities. The acoustoelectric current LAC, which is easier to measure in low resistivity materials, is simply given by LAV/R_t .⁶²

Through the Kramers–Kronig relationship it is well known that the real and imaginary parts of the SAW wave vector are related (causality relationship). Therefore, a change in the imaginary part of the wave vector (i.e., SAW attenuation constant) will result in a change in the real part of the wave vector which means a change in the phase of the SAW. This can be utilized to characterize the semiconductors by measuring the change in the phase of the SAW which can be monitored using homodyning or by using the SAW delay line as an oscillator and monitoring its resonant frequency.¹⁴

The attenuation constant α , of the SAW propagating under the semiconductor in the separate medium convolver is given by^{14,28}

$$\frac{\alpha}{k} = -\frac{K^2}{2} \operatorname{Im} \left[\frac{1 + j\epsilon_0 V_s Z_A}{1 - j\epsilon_p V_s Z_A} \right], \quad (7)$$

where k is the SAW wave vector, K is the electromechanical coupling constant, ϵ_0 is the dielectric constant of the free space, and Z_A is the adjacent medium impedance given by³

$$Z_A = \frac{Z_s + j \tanh(kh)/V_s \epsilon_0}{1 - jV_s \epsilon_0 Z_s \tanh(kh)}, \quad (8)$$

where h is the gap between the semiconductor and the delay line, and Z_s is the TM wave impedance of the semiconductor surface which, in the case of extrinsic n -type semiconductor, is given by^{3,14}

$$Z_s = \frac{\epsilon_0}{\epsilon_s} \left[j \frac{\omega^2}{\omega_{cn}^2} - \frac{\omega}{\omega_{cn}} \left(1 + \frac{1}{\delta} \right) - \frac{j}{\delta} \right] \left[\frac{\omega^2}{\omega_{cn}^2} + 2j \frac{\omega}{\omega_{cn}} - 1 \right], \quad (9)$$

where δ is given by^{3,14}:

$$\delta^2 = \left(1 + \frac{\omega_{cn} \omega_{dn}}{\omega^2} - j \frac{\omega_{dn}}{\omega} \right). \quad (10)$$

The change in the phase of the SAW is usually denoted by $\Delta k_0/k$, where k is the wave vector, and it is given by^{3,14}:

$$\frac{\Delta k_0}{k} = -\frac{K^2}{2} \operatorname{Re} \left[\frac{1 + j\epsilon_0 V_s Z_A}{1 - j\epsilon_p V_s Z_A} \right]. \quad (11)$$

Therefore, a semiconductor can be characterized by either measuring the SAW attenuation or its phase change. Using resonator structure, which can be easily constructed by providing appropriate feedback between the input and output transducers of a SAW delay line, the change in the SAW phase can be monitored by monitoring the change in the oscillator's natural frequency. This is a very accurate way of measuring semiconductor properties.

As mentioned before, the electric field that accompanies the SAW, decays exponentially (with a decay constant of a SAW wavelength) above the surface of the piezoelectric material in the free space. When a semiconductor is placed at the surface of the piezoelectric delay line, this electric field

extends into the semiconductor and within one SAW wavelength or a Debye length, depending on which one is shorter, it becomes negligible. Therefore, the spatial resolution of the SAW technique is on the order of the SAW wavelength or the Debye length, whichever is shorter.

IV. TAV SPECTROSCOPY: IMPURITY LEVELS

The basis of the TAV spectroscopy is that the TAV is a measure of the carrier density within the depth of acoustoelectric interaction in the semiconductor.^{39,41,49,63} TAV spectroscopy is similar to photoconductivity spectroscopy where allowed band-to-band or impurity level-to-band transitions alter the conductivity of the sample and, therefore, are detected.⁶³ In the TAV spectroscopy, due to the fact that the TAV signal is negative for the p -type surface and it is positive for the n -type surface, the conductivity type at different incident photon energies can also be determined.⁶³

TAV spectroscopy can be performed at different temperatures,^{63,67,72} under different dc bias conditions,⁴⁹ and using a second light as a bias light.^{39,41}

The effect of temperature on the TAV amplitude and waveform is discussed in Refs. 63, 67, and 72. As the temperature is changed, the Fermi level changes as a result of the temperature dependencies of the free energy of impurity levels, the semiconductor bandgap energy and the effective density of states. However, in the temperature ranges that are usually used ($300 \text{ K} > T > 77 \text{ K}$) only the concentration of the ionized deep impurities changes and the shallow impurities remain completely ionized.

The experimental set up is shown in Fig. 2. The TAV is monitored while changing the wavelength of the incident photon with or without an applied dc bias voltage (field effect) at different SAW power levels.⁶³ Field-effect measurements are described in the next section. The illumination is directed at the surface on the semiconductor where the AEI takes place. In two-beam spectroscopy,^{39,41,63} a second bias light is used to selectively populate or depopulate impurity levels. Low temperature measurements were performed by placing the delay line box to the cold-head of a cryogenic system.^{57,63,67} In some of the experiments the TAV spectroscopy is performed while using a dc bias voltage to change the surface conditions to increase the sensitivity of the measurement.⁴⁹ In measurements reported here, a Baush and Lomb monochromator was used for the bias beam and a high resolution (1 \AA) Jobin Yvon HRS2 monochromator was used to obtain the TAV spectrum.

TAV spectroscopies have been extensively performed in the past to characterize variety of semiconductors and their interfaces. The most important studies include the detection of bulk and bound excitons in GaAs,^{41,63} characterization of the interface between the GaAs and its anodic oxide,^{39,42,57,63} liquid junction solar cells,³¹ and detection of impurity levels in GaAs,^{39,42,57,63} InP,⁶⁴ InAs,³⁴ CdS,³¹ Si,⁴⁹ $\text{Hg}_{1-x}\text{Cd}_x\text{Te}$ / CdTe ,^{44,47,50} and $\text{Al}_{1-x}\text{Ga}_x\text{As/GaAs}$ ^{54,55,66} quantum wells and superlattices. Here we only report some results on $\text{Al}_{1-x}\text{Ga}_x\text{As/GaAs}$ quantum wells,^{54,55} and $\text{Hg}_{1-x}\text{Cd}_x\text{Te/CdTe}$.

Figure 6 shows the TAV spectrum of a single, metal-organic chemical vapor deposited quantum well having

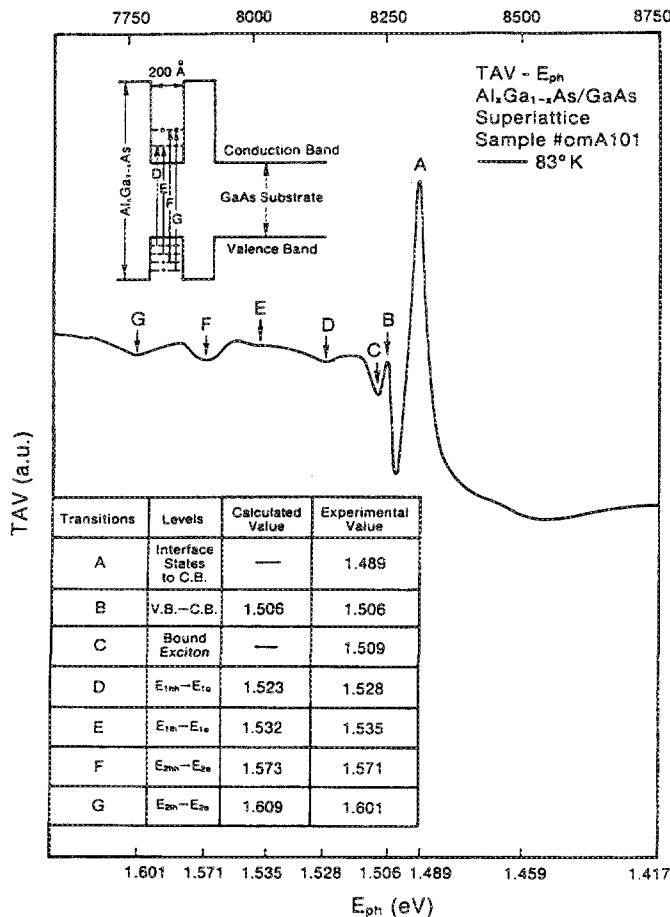


FIG. 6. TAV spectrum for an $\text{Al}_x\text{Ga}_{1-x}\text{As}/\text{GaAs}$ at 83 K.

$\text{Al}_{0.3}\text{Ga}_{0.7}\text{As}(n^+)/\text{GaAs}(200 \text{ \AA})$ structure.^{54,66} Different structures in the TAV spectrum correspond to various inter-band sublevel transitions. "A" is the interface state to bulk conduction band band transition. "B" is due to the large penetration depth of the photons having the band-gap energy (E_g). "C" is due to the bound exciton formation in the bulk. "D"—"G" are due to the valence to conduction band sublevel transitions shown in Fig. 6 inset.⁵⁴ Also shown in that inset is a table that shows the calculated and experimental values of transition energies. The agreement is better than one percent.⁵⁴

Once an impurity level is detected, its radial distribution can also be obtained by monitoring the TAV amplitude as a function of the spatial position of the incident beam with an appropriate fixed wavelength. This technique was used to obtain the spatial distribution of EL2 level in GaAs.⁶³

SAW power is also used as an additional parameter in TAV spectroscopies. It is used to break exciton bonds in the GaAs and it is observed that it has a pronounced effect on the TAV spectrum.⁶³ Figure 7 shows the effect of the SAW power on the $\text{Hg}_{1-x}\text{Cd}_x\text{Te}/\text{CdTe}$, TAV spectrum. At high SAW powers, the AEI takes place between the SAW and mainly CdTe substrate.⁴⁴ Therefore, the TAV spectrum at SAW powers does not exhibit structures due to electronic transitions in the $\text{Hg}_{1-x}\text{Cd}_x\text{Te}/\text{CdTe}$ system. By performing the spectroscopy at low enough SAW power level, these

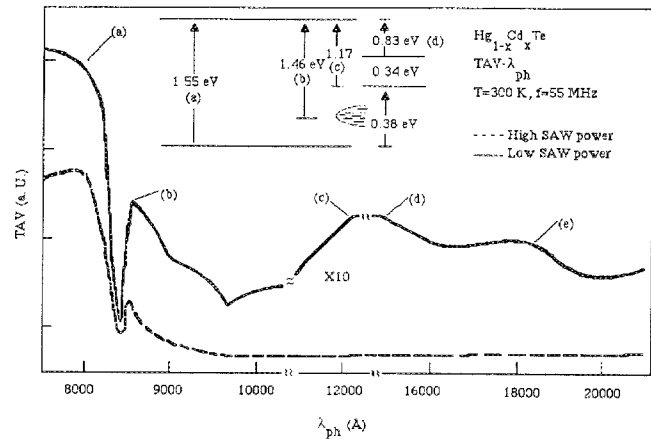


FIG. 7. Experimental TAV- λ_{ph} plot for epitaxial $\text{Hg}_{1-x}\text{Cd}_x\text{Te}$ on CdTe. Different transitions are shown in the inset.

transitions are observed and are used to estimate the band-gap and, thus, the alloy composition (x) of the $\text{Hg}_{1-x}\text{Cd}_x\text{Te}$ sample and the band offset between the CdTe substrate and $\text{Hg}_{1-x}\text{Cd}_x\text{Te}$ epitaxial layer.^{44,47}

The theoretical treatment of SAW/semiconductor interaction, that was briefly described in Sec. III, is based on linearized partial differential equation of the potential inside the semiconductor. In reality, the presence of SAW electric field alters the surface carriers' concentrations and the linearized theory developed so far is inherently unable to explain the effect of SAW power on the TAV spectrum.

The TAV spectrum at low SAW power is used to estimate the bandgap and, thus, the alloy composition (x) of the $\text{Hg}_{1-x}\text{Cd}_x\text{Te}$ sample. Figure 7 shows that there are transitions around 8000 Å [1.55 eV; transition (a)], 8550 Å [1.45 eV; transition (b)], 10 000 Å [1.24 eV; transition (c)], 15 000 Å [0.827 eV; transition (d)], and 18 000 Å [0.689 eV; transition (e)]. These transitions, shown in Fig. 7 inset, indicate that the HgCdTe band gap should be around 0.34 eV. At $T = 300 \text{ K}$, the energy gap of 0.34 eV corresponds to the x value of 0.33.

V. FIELD EFFECT MEASUREMENTS: DETERMINATION OF INTERFACE TRAP DENSITIES AND CARRIER DENSITY PROFILE

A. Interface trap density and flatband voltage

Using field effect measurements, flat band voltage,^{44,48} interface trap density as a function of energy,^{49,53,75} and carrier density profiles^{40,42} are obtained. Figure 8 shows a LiNbO_3 delay line used in performing the field effect measurements. A 5000 Å aluminum film is deposited at the surface of the piezoelectric delay line. This is used to change the surface potential of the semiconductor via field effect. To provide openings for the acoustoelectric interaction, 50–100 μm diam interaction windows are defined using photolithography on the aluminum film. The electric field of the SAW interacts with the semiconductor through these window openings. Also to prevent any dc current conduction through the semiconductor, 1000 Å of Al_2O_3 is anodically grown over the ground aluminum path.⁴⁹

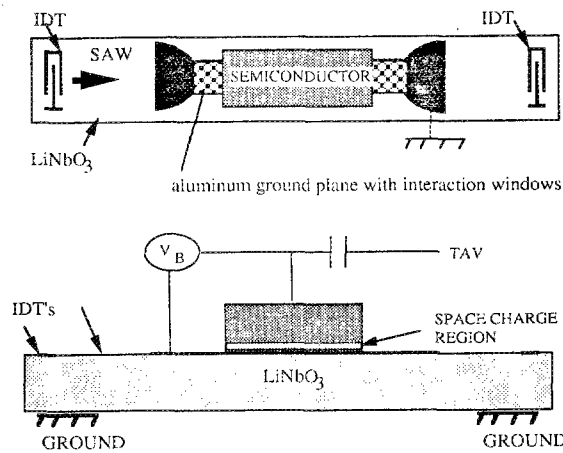
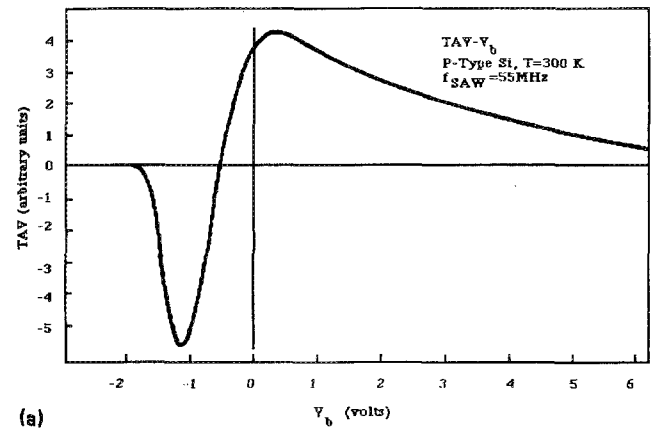


FIG. 8. The delay line used in TAV as a function of applied bias field measurements. The ground plane in an aluminum thin film covered with Al_2O_3 with $100\text{ }\mu\text{m}$ interaction windows.

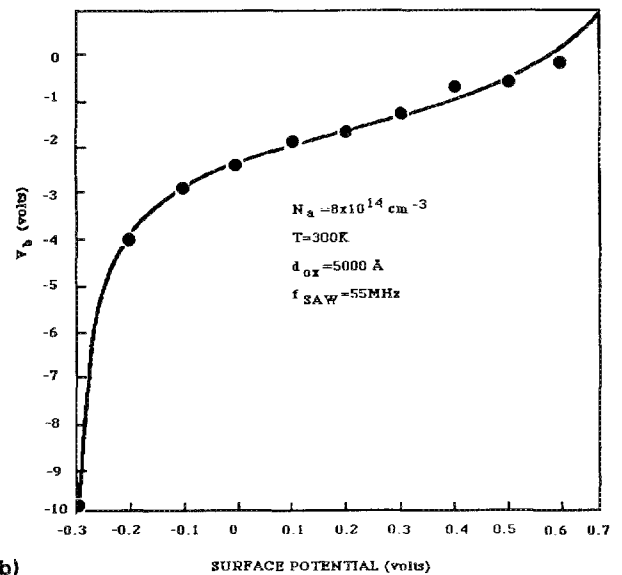
The dc bias field is applied to the surface of the semiconductor as shown in Fig. 8. Due to the nearly ohmic nature of the back contact, the space charge region is mainly generated at the surface of the semiconductor. The space charge region also extends laterally over the interaction windows where the acoustoelectric interaction takes place. Therefore, by changing the bias voltage the carrier concentration over the interaction window is effectively modulated and the TAV as a function of the applied bias ($\text{TAV}-V_b$) or the surface potential ($\text{TAV}-\Psi_s$) is obtained. The fixed oxide charge density (Q_{ox}), flatband voltage (V_{FB}), and interface trap density versus the interface trap energy ($D_{it} - E_{it}$) are then obtained by comparing the experimental $\text{TAV}-V_b$ with the theoretical TAV versus surface potential curves. This procedure is similar to the high frequency capacitance versus voltage ($C-V$) technique.

A typical experimental $\text{TAV}-V_b$ of Si/SiO₂ system is shown in Fig. 9(a). The experimental and theoretical (not shown here) curves are normalized to have the same maximum. At any given TAV, the V_b and Ψ are read from the corresponding axis of the experimental and theoretical curves, and a $V_b-\Psi$ curve is constructed.⁵³ Figure 9(b) shows the resultant $V_b-\Psi_s$ curve. The $(D_{it}-E_{it})$ is evaluated from the slope of $V_b-\Psi_s$ curve exactly like in the $C-V$ case.^{44,53} Figure 10 shows the resultant $D_{it}-E_{it}$ curve. The V_{FB} is determined from the value of the V_b that corresponds to $\Psi_s = 0$. The disagreement between the TAV and $C-V$ results is due to the nonuniformity of the semiconductor surface potential over the interaction window. This nonuniformity can be taken into account in the calculation. We have observed that by making the interaction windows smaller than the TAV and $C-V$ results agree better with each other. As the windows are made smaller the TAV amplitude diminishes. Ultimately the signal to noise ratio determines the smallest interaction window that can be used at any given SAW frequency.

Si/SiO₂,⁵³ HgCdTe/ZnS,^{44,47} and GaAs/(Ga₂O₃,As₂O₃)⁶³ interfaces have so far been studied. In the



(a)



(b)

FIG. 9. (a) The experimental $\text{TAV}-V_b$ for a p -type boron doped Si sample. (b) The bias voltage V_b as a function of surface potential (Ψ_s) curve derived using (a) and the theoretical $\text{TAV}-\Psi_s$ curve.

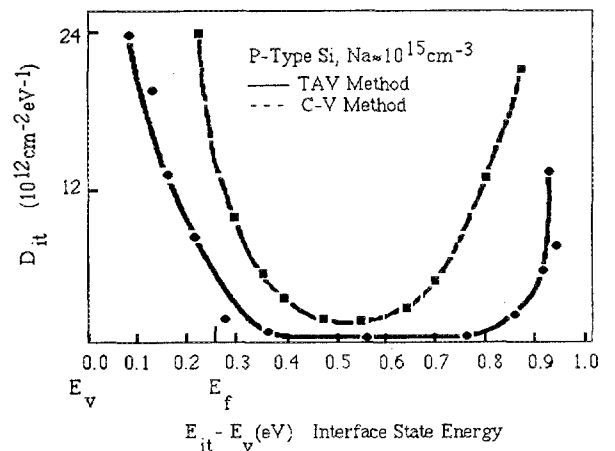


FIG. 10. The interface trap density vs interface trap energy curves calculated using the V_b vs Ψ_s shown in Fig. 9(b).

case of Si/SiO₂, which is the most extensively studied system, the findings of the SAW technique was compared with the results of the capacitance versus voltage measurements and satisfactory quantitative agreement were observed.⁵³ There has been also some recent measurement on Si/SiO₂ system showing changes in $D_{it}-E_{it}$ as a function of pressure.^{68,75}

B. Carrier density profile

To obtain the majority carrier profile the effective carrier density at a given bias voltage is calculated by comparing the experimental TAV- V_b curve with the theoretical TAV versus carrier density curves (TAV- n).^{40,42} These two curves are normalized to have the same maximum, and at a given TAV amplitude, the values of n and V_b are obtained from the corresponding axis in a manner similar to interface trap density determination. Thus, $n(V_b)$ is constructed and the depletion width as a function of the applied bias voltage $W(V_b)$ is determined from $n(V_b)$ using the Poisson's relationship in a finite difference form. Then, the doping profile $n(W)$ is found from $n(V_b)$ and $W(V_b)$ curves. Figure 11 shows a typical doping profile of the implanted region in silicon. This result is preliminary and it compares satisfactorily with the results expected from the ion implant dose and energy. The advantage of using SAW for carrier density profiling, in addition to its nondestructive nature, is its very high sensitivity for low concentration of the implant.^{40,42}

VI. GENERATION/RECOMBINATION LIFETIMES

A. Carrier lifetime in materials

The SAW is usually pulsed to enable capacitive detection of acoustoelectric voltages or to be able to measure the SAW attenuation. Thus, there are transients associated with the measure signals.^{46,51,67} The time constant associated with these transients, which are usually exponentials, are related

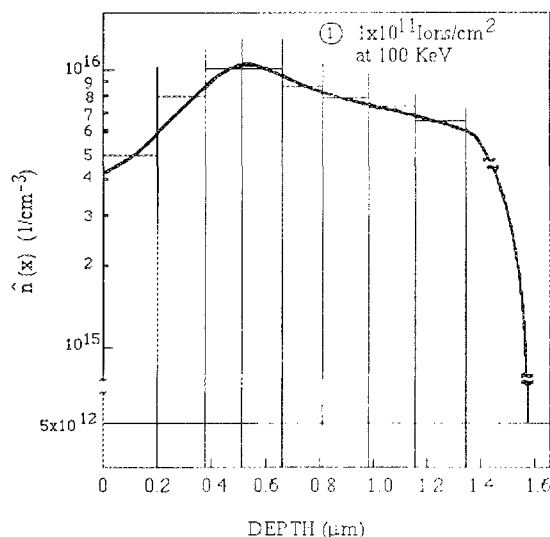
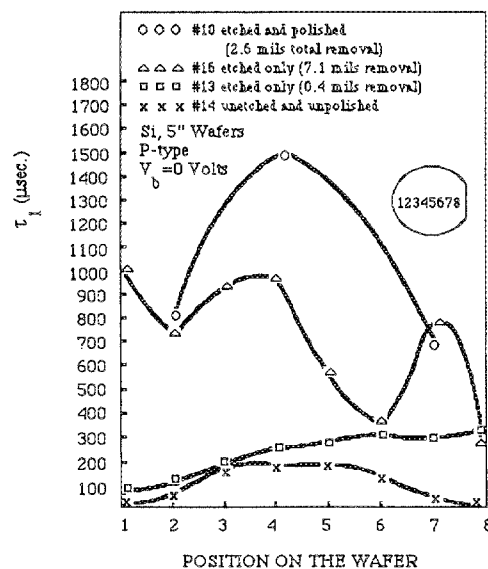


FIG. 11. Experimentally determined majority carrier density profile for a phosphorus implanted (phosphorus) silicon sample.

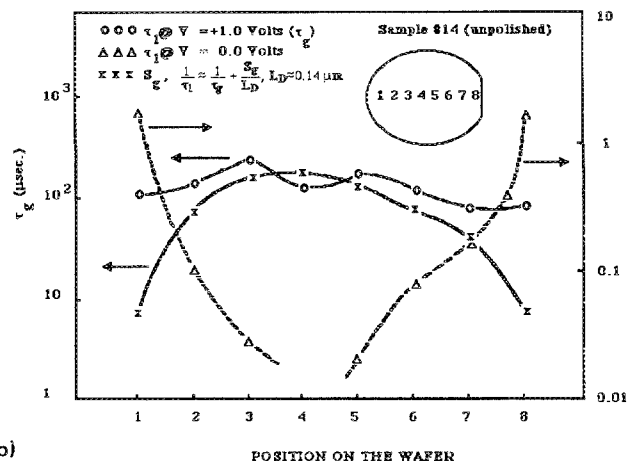
to the capacitive response time of the separate medium structure,⁶⁷ the response time of the instrumentation, and the response time of the carriers in the semiconductor.^{46,51,67} Especially in the case of high resistivity samples with depleted surfaces, the generation lifetime of the carriers (majority and minority carriers depending on the relative position of the Fermi level with respect to the midgap energy) can dominate the TAV rise time. The relationship between the TAV transient (τ_1 in Fig. 3) and the generation lifetime is discussed in Refs. 46, 51, and 67. Near flat band conditions, τ_1 is given by

$$\frac{1}{\tau_1} = \frac{1}{\tau_g} + \frac{S_g}{L_D}, \quad (12)$$

where τ_g is the carrier generation lifetime, L_D is the extrinsic Debye length and S_g is the surface generation velocity. The separation of τ_g and S_g is possible by the application of a



(a)



(b)

FIG. 12. Carrier lifetime distribution across p -type, boron doped, silicon samples with different surface conditions. (b) Surface generation velocity and minority carrier generation lifetime across an unpolished p -type boron doped silicon wafer.

depleting dc bias field to the surface of the semiconductor.⁴⁶ In these measurements, τ_1 as a function of voltage ($\tau_1 - V_b$) is obtained. Figure 12(a) shows the spatial variation of τ_1 across Si samples.⁴⁶ The plots indicate a large spatial variation of τ_1 with generally lower values towards the edge. By performing $\tau_1 - V_b$ measurements it is demonstrated that the surface effect due to nonzero S_g can be reduced under depleting bias fields. Thus, the spatial distribution τ_g and S_g was obtained as shown in Fig. 12(b).^{46,51} Above technique is used to determine the carrier generation lifetime in Si,^{46,51} and GaAs.⁶⁷

B. Carrier lifetime in diode arrays

It is also possible to charge the interface traps of diode arrays and to monitor the subsequent decay of the charges by recording the convolution voltages.⁵⁸ Figure 13 shows the experimental set-up used in this case. Two rf pulses with amplitudes of A_1 and A_2 are sent to transducers No. 1 and No. 3. When $A_2 \gg A_1$, the superposition of these two surface waves result in the following wave⁵⁸:

$$E_s = \sqrt{[A_2(t + z/v) + A_1(t - 1/v)\cos 2kz]} \times \sin[\omega t + \phi(z)]. \quad (13)$$

The positive rf cycle of the standing wave forward biases the diodes and given sufficient time, a peak detection occurs and the stored charge distribution follows the maximum amplitude of the standing wave. Once the charge grating is written-in, the standing wave is turned off. Hence, the charges stored within the diffusion capacitances, reverse biases the diodes and because of the very low conductivity of reversed biased $p-n$ junction, these charges decay very slowly. A convolution of an rf pulse at 2ω (having a wave vector $2k$), that is applied to transducer No. 2, with the charge grating in the array is used to monitor the charge content of the $p-n$ diodes. By monitoring these charges as a function of time, their decay constant is determined. In Ref. 58 the effect of TAV and

LAV on the charge content of the $p-n$ diode arrays is discussed. Figure 14(a) shows the rf pulse and its convolution with the information stored in the diode array. Figure 14(b) shows the decay of the convolution signal as a function of time after the standing wave is turned off. Using this technique, the charge storage capability of the $p-n$ diode array is determined.

Carrier lifetime is an important device parameter that is significantly affected by material quality. Therefore it is measured to assess the effect of fabrication steps on the material quality and also it is used in device modeling. It is demonstrated that the SAW technique is capable of quantitatively determining this important parameter.^{46,51,58,67}

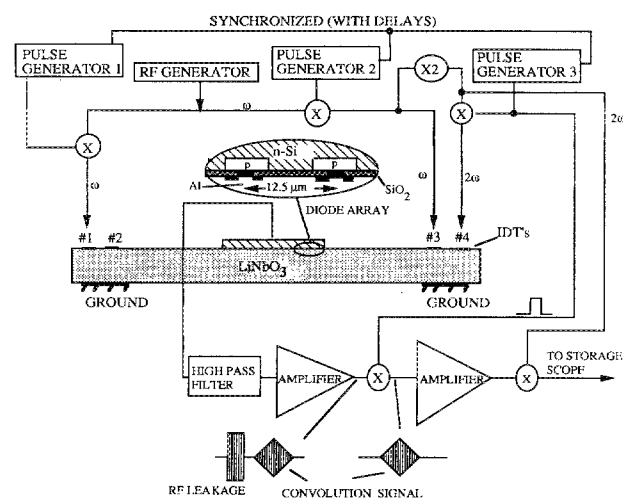
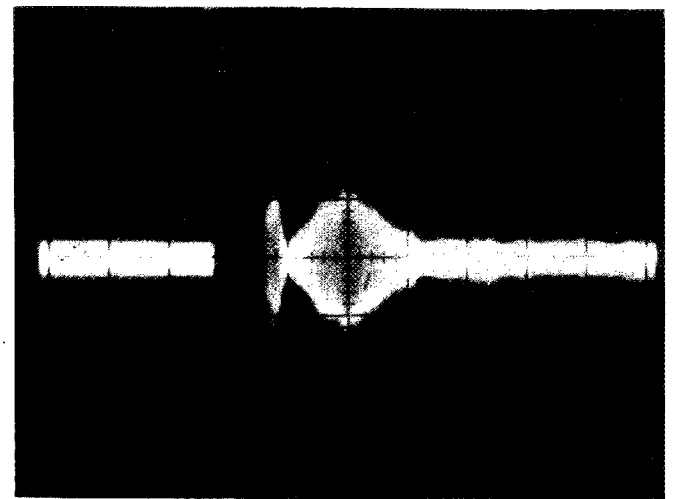
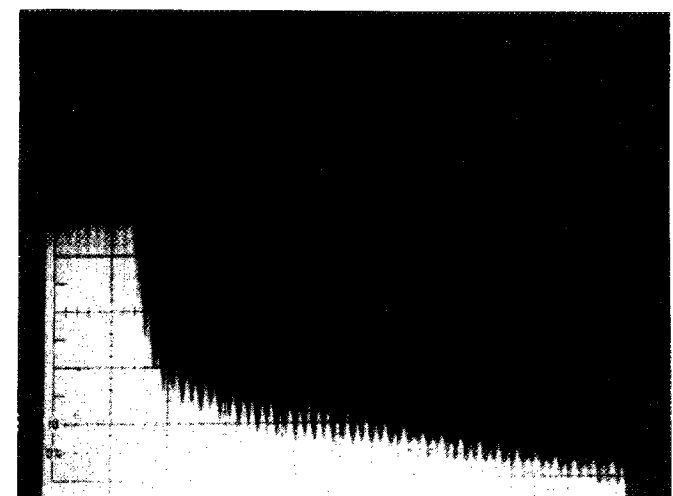


FIG. 13. The experimental set-up to characterize diode arrays using the convolution signal.



(a)



(b)

FIG. 14. (a) The read-out (2ω) and convolution signals. The vertical scale is 1 V/div. for the read-out signal and 0.01 V/div. for the convolution signal. The time scale is 2 μ s/div. (b) The decay of convolution signal as a function of time after the write-in pulse (standing wave) is turned off (1 V/div. and 20 ms/div.).

VII. THERMALLY STIMULATED TAV MEASUREMENTS: DEEP LEVELS

It is well known that deep levels play an important role in the operation of $\text{Al}_x\text{Ga}_{1-x}\text{As}/\text{GaAs}$ -based high electron mobility transistors, photodetectors, and light modulators. More specifically, deep levels acting as carrier traps deteriorate the dc bias stability of these devices and limit the impulse response of detectors. Deep levels and their properties are also important parameters in characterizing the material quality.

In the majority of deep-level measurements, a trap state inside the semiconductor band gap is filled by an external stimulus, such as an externally applied voltage across a metal-oxide-semiconductor (MOS) structure or an optical pulse directed at the depletion region of a MOS diode. After the external stimulus is removed, the traps emit their charges to move toward their equilibrium state. The rate of emission of charges depends on the trap-state parameters that are themselves temperature dependent. These transients, therefore, are recorded as a function of temperature to extract trap parameters.

In the SAW technique the transients are studied by directly monitoring the carrier type and concentrations within a few micrometers (depending on the wavelength of SAW and the carrier concentrations) depth of the surface. Also, the sensitivity of the SAW measurement becomes larger as the resistivity of the samples is increased.

The AEI results in an alteration of the carrier density at the surface of the semiconductor. The rate at which these excess charges are induced at the semiconductor surface, or diminished after the passage of the SAW pulse, can be related to the position, the density, and the cross sections of the deep levels inside the bandgap of a high-resistivity semiconductor. The amplitudes and the time constants associated with the TAV waveform are monitored as a function of the temperature to determine the trap parameters.

The SAW rf pulse and the resulting TAV waveform is shown in Fig. 3. At a fixed temperature, τ_1 usually tends to be smaller than τ_2 . This indicates that, when SAW is ON, it increases the dc surface conductivity. In qualitative terms, τ_1 is determined, in addition to other geometric parameters, by how fast the nonlinear current density profile can be established. This requires accumulation of the majority carriers at the surface and their depletion beneath the surface as discussed in Sec. IV (shown in Fig. 4).

When it is assumed that the thermally stimulated carrier concentration reaches a maximum when the Fermi level crosses the trap energy (E_T , measured from the conduction band) and in quasiequilibrium, the trap energy is related to the conductivity peak temperature (T_m) as follows^{67,72}:

$$E_T = 23kT_m, \quad (14)$$

where k is the Boltzmann constant and the factor 23 is calculated using typical values for capture cross sections in GaAs. It should be emphasized that Eq. (14) is an approximation.

Treating the AEI as an excitation that results in the accumulation of the semiconductor surface, the release of the majority carriers from deep levels that lead to the thermal equilibrium has the following dependence on time⁶⁷:

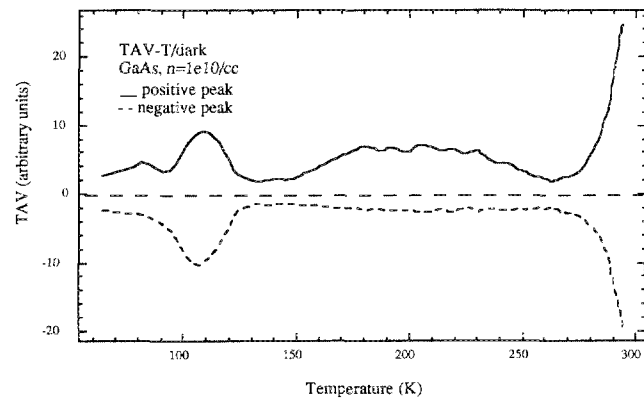


FIG. 15. TAV vs temperature measurements at dark.

$$\Delta n(t) = N_t (1 + \tau_f/\tau_g)^{-1} \exp(-t/\tau_g), \quad (15)$$

where N_t is the trap density of those deep levels near the Fermi level, τ_f is the time constant associated with the filling rate of these levels in the presence of the external stimulus, and τ_g is the time constant associated with the release of the carriers from deep levels once the external stimuli is turned off. τ_g has the following temperature dependence⁶⁷:

$$\tau_g^{-1} = \gamma_n T^2 \sigma_{na} \exp(-E_n/kT), \quad (16)$$

where $\gamma_n = 2.28 \times 10^{20} \text{ cm}^{-2} \text{ s}^{-1} \text{ K}^{-2}$ for electron traps in GaAs, σ_{na} is the apparent cross section, and E_n is trap energy from the conduction band. Since the TAV signal is detected through a high-pass filter (essentially a differentiator), the amplitude of the detected signal also reflects the TAV transient time constants.

Figure 15 shows an example of the TAV versus temperature (TAV-T) curve that is obtained for a GaAs sample without any illumination. Under illumination some peaks in the the TAV-T are observed.⁶⁹ Using Eq. (14) and the values for the temperatures at which TAV maximum occurs in the TAV-T curves, Table I displays the activation energies calculated for Cr-doped GaAs.^{69,72}

Figure 16 shows the variation of the TAV rise times (τ_1 and τ_2 , shown in Fig. 3) as a function of temperature at dark across a $\text{Al}_x\text{Ga}_{1-x}\text{As}/\text{GaAs}$ material grown by molecular beam epitaxy. The substrate is a semi-insulating CZ grown, undoped, (100) wafer. The first layer is a 12 μm , high quality GaAs buffer layer with 10^{15} cm^{-3} carrier density. The second layer is a 40 \AA $\text{Al}_x\text{Ga}_{1-x}\text{As}$ ($x = 0.3$) spacer which is followed by a 400 \AA Si-doped $\text{Al}_x\text{Ga}_{1-x}\text{As}$ ($x = 0.3$)

TABLE I. Calculated activation energies for Cr-doped GaAs (Refs. 69 and 72).

Bias light (eV)	Trap energy (eV)	Nature of the trap
none	0.6	Electron trap
0.99	0.37	Hole trap
1.38	0.184	Electron trap
white	0.32	Electron trap

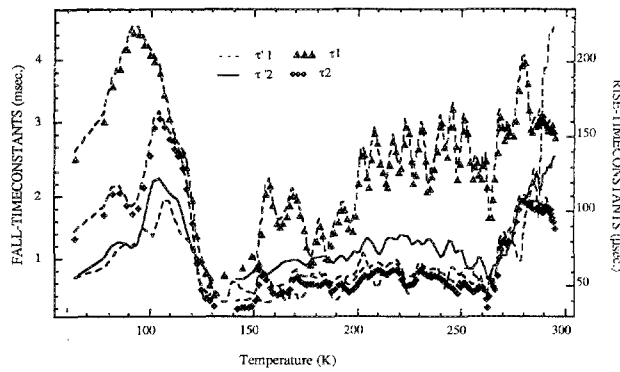


FIG. 16. Transient time constant as a function of temperature measurements at dark. For definition of various time constants please refer to Fig. 3.

layer with doping density of $2 \times 10^{18} \text{ cm}^{-3}$. This is followed by a 10^{18} cm^{-3} Si-doped, 400 Å, GaAs cap layer. The TAV- T and τ - T measurements were also performed under 1.38 and 1.49 eV illuminations. The effect of SAW power on the τ - T measurements were also extensively studied.^{63,67,69} The activation energies and trap cross sections, summarized in Table II, were calculated using Eqs. (15) and (16).

VIII. DETERMINATION OF CARRIER MOBILITY USING ACOUSTOELECTRIC MEASUREMENTS

To determine the carrier mobility, the delay line shown in Fig. 17 is used and LAV is measured as a function of absorbed SAW power (P_{abs}). The relationship between LAV and P_{abs} is given by Eq. (6). P_{abs} is usually determined by measuring the output SAW power at the second transducer with and without the semiconductor being present.^{21,62}

TABLE II. Activation energies and apparent cross sections.

E_n (eV)	σ_{na} (cm ²)	
At dark	0.15	4×10^{-19}
	0.18	3×10^{-18}
	0.21	8×10^{-19}
	0.27	1×10^{-17}
	0.32	5×10^{-16}
	0.4	1×10^{-20}
	0.41	2×10^{-15}
	0.9	7×10^{-6}
Under 1.49 eV ill.	0.14	4×10^{-19}
	0.15	4×10^{-19}
	0.17	8×10^{-19}
	0.83	2×10^{-19}
Under 1.38 eV ill. SAW = 9V _{pp}	0.12	8×10^{-20}
	0.25	1×10^{-17}
	0.37	1×10^{-15}
	0.37	4×10^{-16}
	0.6	5×10^{-12}
	Under 1.38 eV ill. SAW = 20 V _{pp}	0.11
0.16		2×10^{-20}
0.24		6×10^{-17}
0.34		7×10^{-16}
0.36		9×10^{-16}

There is also an alternative scheme that calculates the root mean square of the electric field (E_{ac}) at the semiconductor surface, and in the case of high resistivity materials where absorbed SAW power per unit length (P_{abs}/L) can be small and constant, it relates P_{abs}/L to E_{ac} through the resistance of the semiconductor.³³

LAV measurements are used for high resistivity semiconductors.⁶² In the case of low resistivity materials such as $\text{Hg}_{1-x}\text{Cd}_x\text{Te}$, the longitudinal acoustoelectric current (LAC) is more conveniently measured.⁶²

Since TAV is much more convenient to measure than the longitudinal signals, a relationship between TAV and carrier mobility can also be derived⁶²:

$$\text{TAV} = \frac{P_{\text{av}} \alpha'}{\epsilon_0 \omega V_s} \mu_n, \quad (17)$$

where α' and P_{av} (the average SAW power) are defined in Fig. 17, ω is the SAW frequency, and ϵ_0 is the permittivity of the free space.

The recent advances in using SAW to measure the carrier mobility are the use of field effect to change the surface conductivity type to measure the minority carrier mobility and also to use TAV measurement instead of LAV or LAC measurements. Carrier mobility in a variety of semiconductors including Si, CdTe, hydrogenated amorphous $\text{Si}_{0.6}\text{Ge}_{0.4}$, GaAs, and, more recently, $\text{Hg}_{1-x}\text{Cd}_x\text{Te}$ are measured using the SAW technique.

Figure 18 shows a typical LAV versus P_{abs} curve obtained across a $\text{Hg}_{1-x}\text{Cd}_x\text{Te}/\text{CdTe}$ sample at $T = 77 \text{ K}$.⁶² Figure 19 shows the mobility profile as a function of etching of the surface of the above sample in 5% bromine methanol which has a etch rate of 600–900 Å/min at $T = 300 \text{ K}$. Right at the surface the conductivity is n -type with electron mobility of $190 \text{ cm}^2/\text{V s}$ (determined from the slope of LAV versus P_{abs}

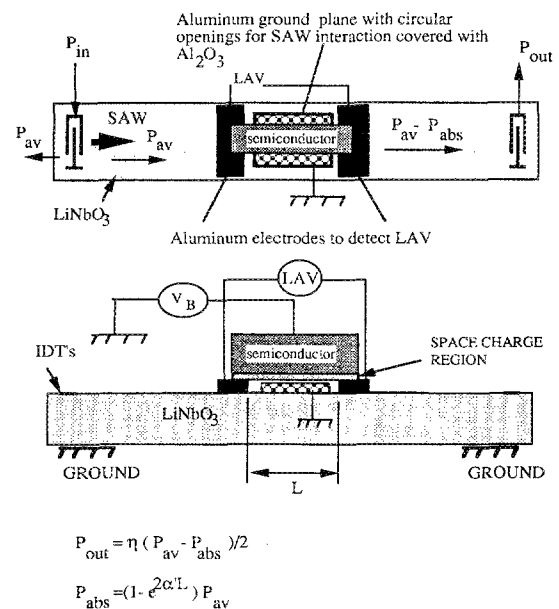


FIG. 17. The LiNbO_3 delay used in LAV as a function of absorbed SAW power and applied bias measurements.

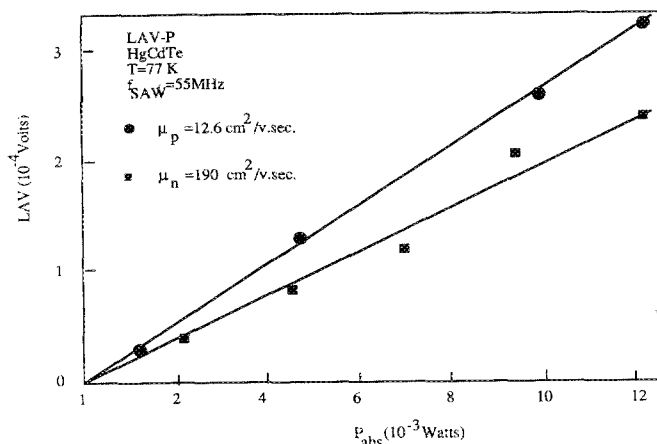


FIG. 18. The LAV as a function of SAW power for a $\text{Hg}_{1-x}\text{Cd}_x\text{Te}$ sample. This measurement is performed before (squares) and after (circles) etching the sample for 20 s in 5% Br methanol.

shown in the Fig. 18), and after 10 s of etching (depth of around 100–150 Å) the conductivity becomes p -type with a hole mobility of less than $10 \text{ cm}^2/\text{V.s}$. The carrier type is determined from the polarity of the acoustoelectric voltages as discussed before. The quantitative agreement these findings and Hall measurement results on the same sample were satisfactory.⁶²

In the case of $\text{Hg}_{1-x}\text{Cd}_x\text{Te}/\text{CdTe}$, the surface condition is quite unstable. The surface conductivity changes unpredictably through the fabrication sequence and sometimes even by itself only due to the exposure to the environment, and a nondestructive technique such as SAW can be quite beneficial to monitor the evolution of the surface characteristic and to reject the unacceptable wafers early in the fabrication to save time and valuable resources.

IX. RECENT ADVANCES AND TRENDS

In this section some very interesting results and phenomena that are only recently reported are discussed.

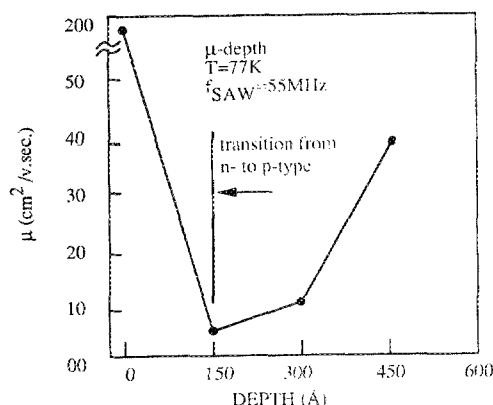


FIG. 19. The variation of mobility as a function of depth in a $\text{Hg}_{1-x}\text{Cd}_x\text{Te}/\text{CdTe}$ sample. This figure is obtained after successively etching the surface in 5% Br methanol.

A. AEI in superlattices

Figure 20 shows the rf pulse (trace a) that is used to generate the SAW and the TAV signal that is detected across a superlattice consisting of 80, symmetric cells of GaAs/AlAs of approximately 45 Å layer thickness, grown by metal-organic chemical vapor deposition (MOCVD).^{54,55} There is low Si doping ($\sim 5 \times 10^{17} \text{ cm}^{-3}$) in the AlAs and the substrate is slightly n -type, semi-insulating, GaAs. The complete reversal of the polarity of TAV waveform of the superlattice at two different frequencies (55.70 and 55.68 MHz) is shown in Fig. 20, traces b and c.

The SAW frequency dependencies of TAV for bulk semiconductor (GaAs) and the superlattice (GaAs/AlAs) are shown in Fig. 21. The TAV of the superlattice, on the other hand, exhibits drastic variation as a function of SAW frequency ($\Delta f_{\text{SAW}} \sim 10 \text{ KHz}$). It should be noted that at certain frequencies the polarity of TAV changes (Fig. 21) sign, a phenomena that is not observed in the bulk semiconductor. Similar oscillations as a function of SAW frequency also have been observed in the LAV. This behavior of the TAV as a function of SAW frequency is attributed to the generation of acoustic waves in the layered, dispersive superlattice structure.

There are some theoretical studies that have been carried out to explain and understand the AEI in layered structures.^{38,56,59,65} The preliminary results on single quantum wells are quite interesting. More work is needed in order to achieve satisfactory understanding of the acoustoelectric phenomena in superlattice structures.

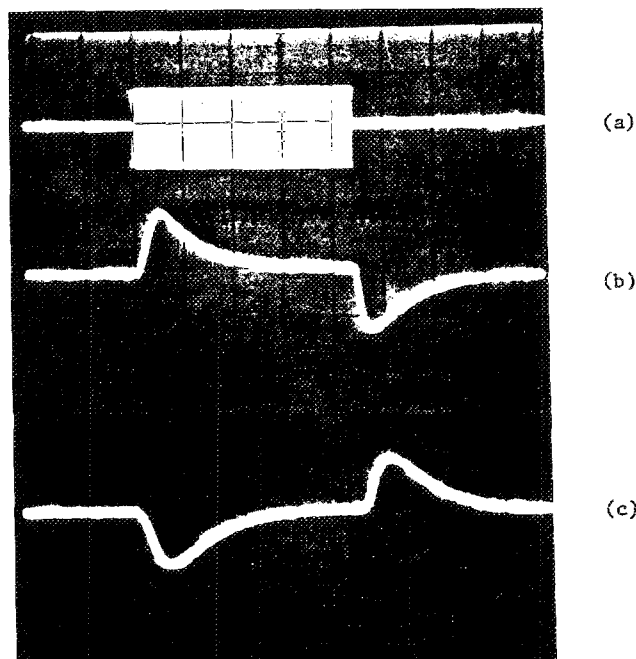


FIG. 20. The rf pulse [trace (a)] and the TAV waveform across the GaAs/AlAs superlattice. Trace (b) and $f_{\text{SAW}} = 55.75 \text{ MHz}$ and trace (c) when $f_{\text{SAW}} = 55.68 \text{ MHz}$. Vertical scales: trace (a) 5 V/div., traces (b) and (c) 0.01 V/div., horizontal scales: 2 ms/div.

B. AEI in superconductors

Figure 22 shows a plot of the magnitude of the TAV signal as a function of temperature in $\text{YBa}_2\text{Cu}_3\text{O}_{7-x}$ superconductor.^{70,71} Reproducible temperature oscillations are observed in TAV as a function of temperature and the TAV signal vanishes abruptly at the transition temperature of 82 K. Around room temperature the polarity of the acousto-electric voltage is negative indicating that holes dominate the acoustoelectric interaction and the conductivity temperature coefficient is positive indicating that the material is semiconductor around room temperature. Below the superconductive transition temperature the acoustoelectric voltage vanishes abruptly. This is used to nondestructively determine the transition temperature of high T_c ceramic superconductors and to monitor whether electrons or holes are dominating the conductivity.

The temperature dependence of the TAV can be understood in terms of the carrier screening length of the superconductor. In the normal state, the free carrier screening length is greater than the wavelength of the electric field accompanying the SAW. Thus the electric field can penetrate a distance of the order of the SAW wavelength ($64 \mu\text{m}$ for SAW frequency of 55 MHz) into the bulk superconductor. The electric field can then interact with the free carriers of the normal state superconductor. This nonlinear electric field-free carrier interaction provides the dc acoustoelectric voltage observed. Below the transition temperature, the free carrier screening length becomes less than the SAW wavelength and thus the electric field is effectively screened from the superconductor and the nonlinear free carrier-electric field interaction is eliminated. Thus no TAV signal is observed below the superconducting transition temperature.

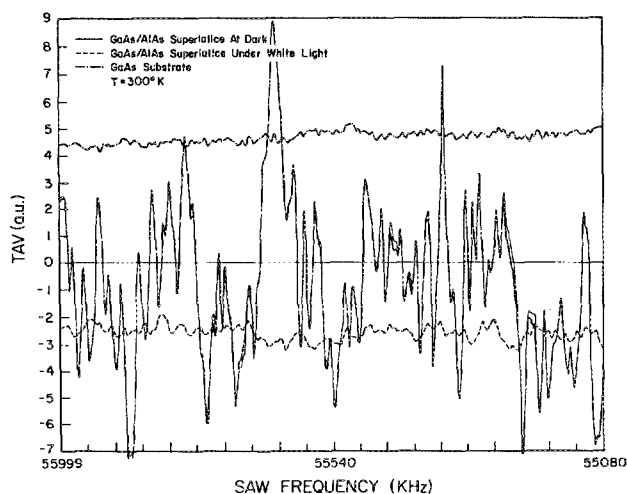


FIG. 21. TAV and SAW frequency ($\text{TAV}-f_{\text{SAW}}$) plot of the GaAs/AlAs superlattice at dark (solid line) and under white light illumination (dashed line). The solid curve is obtained using SAW powers of 80 and 40 mW. The amplification was adjusted to obtain identical TAV amplitude at $f_{\text{SAW}} = 55.68 \text{ MHz}$. The $\text{TAV}-f_{\text{SAW}}$ of GaAs substrate (dot-dashed line) is obtained at dark.

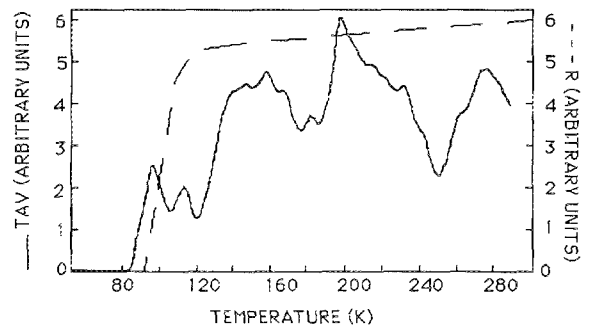


FIG. 22. TAV vs temperature measured across the $\text{YBa}_2\text{Cu}_3\text{O}_{7-x}$ high T_c superconductor (solid line). The superconducting onset is around 90 K. Four point probe resistivity measurement is also included for comparison (dashed line).

C. Anomalous AEV

In the SAW measurements, the propagation plane of the wave is the x - z plane and its direction is the z direction. In the x direction it is assumed that SAW is constant and, therefore, all the derivatives with respect to x are zero. This means that the acoustoelectric signals do not have a component in the x direction. However, in two recent works (one still unpublished) it was reported and confirmed that an acoustoelectric voltage exists in the x direction.⁵²

D. Future trends

In some of the measurements where SAW power was used as an additional parameter, it was shown that by increasing the SAW power the TAV spectrum was not simply increased proportional to the SAW power. It is demonstrated that at higher SAW powers, some of the structures observed in the TAV spectrum are drastically altered or eliminated.⁶³ This requires complete derivation of AEI in a self consistent manner so that the dc alternation of surface carriers due to AEI can be taken into account.

In AEI in the superlattices, it is shown that there are very interesting changes that occur in the TAV as a function of SAW frequency.^{54,55} To understand this phenomena a detailed study of AEI in layered structures is needed. The present treatments are not able to explain the experimental data satisfactorily. Most probably more controlled experiments, in terms of determining what is important and what is not, are needed to help build a theoretical model.

One aspect of the AEI in superlattices is treatment of AEI in non flat-band semiconductors. This is also not yet studied theoretically. Extensive published and unpublished data exist showing the effect of dc biasing on the TAV and also the effect of SAW power on the $\text{TAV}-V_b$.

In $\text{TAV}-V_b$ measurements, the electric field of the SAW interacts with the semiconductor through interaction windows with $50\text{--}100 \mu\text{m}$ diameters. These interaction windows are openings in the aluminum ground plane. The aluminum plane is used to apply a dc electric field to the surface of the semiconductor and to alter its surface conductivity using field effect. Therefore, depending on the window size and the distance between the ground plane and the semiconductor,

only small fraction of the semiconductor surface is affected by the dc electric field. Despite this, it is possible to invert the semiconductor surface as shown in Fig. 9(a). Therefore, the dc field effect should be viewed differently when the SAW electric field is present. This process is not studied yet. A somewhat more accurate model for the AEI has been presented taking into account the effect of trapped charges at the surface of the semiconductor. Experiments^{74,75} pointed out that charge trapping can affect the AEI, therefore this model can be useful to explain some of the experimental results.

A very interesting area that recently has received a renewed attention is SAW gas sensors, corrosion studies, and polymer and organic material characterization. In majority of these studies coated SAW oscillators typically operating in the 10 MHz–1 GHz range are used. Very interesting studies are performed to study diffusion process in polymers and other organic materials. For a in depth review of this upcomming field references 76–80 should be consulted.

X. CONCLUSIONS

We have shown that SAW technique can be used as a powerful tool for studying the electrical properties of semiconductors. In particular within the past eight years, a good number of techniques incorporating the AEI in separate medium configuration have been introduced and used to quantitatively study semiconductors and, more recently, high T_c superconductors. Important semiconductor parameters such as carrier density, carrier type and mobility, interface and fixed oxide charge densities, deep-level cross-section and activation energy, and excess carrier generation and recombination lifetimes are all determined using SAW. A large variety of semiconductors were characterized using SAW including: silicon, GaAs, $\text{Al}_x\text{Ga}_{1-x}\text{As}$, InAs, GaP, $\text{Hg}_x\text{Cd}_{1-x}\text{Te}$, CdTe, InP, CdS, and InAs. The most important aspect of the SAW technique is that it is nondestructive and it is very sensitive for studying high resistivity materials.

¹Kratzig, Solid State Commun. **9**, 1205 (1971).

²(a) D. L. White, J. Appl. Phys. **33**, 2547 (1962); (b) R. M. White and S. M. Volmer, Appl. Phys. Lett. **8**, 40 (1966).

³K. L. Lakin and H. J. Shaw, IEEE Trans. Microwave Theory Techniques **MTT-17**, 912 (1969).

⁴K. A. Ingebrigtsen, J. Appl. Phys. **40**, 2681 (1969).

⁵O. W. Otto, J. Appl. Phys. **45**, 4373 (1974).

⁶S. Datta and B. J. Hunsinger, J. Appl. Phys. **49**, 475 (1978).

⁷M. Hoskins, F. Fliegel, S. Mahon, S. Datta, and B. J. Hunsinger, 1980 IEEE Ultrasonic Symposium Proceedings (IEEE, New York, 1980), Pub. No. 80CH1602-2, Vol. 1, p. 142.

⁸V. Norayanamurti, H. Halstormer, M. A. Chin, A. C. Gossard, and W. Wenzmann, Phys. Rev. Lett. **27**, 2012 (1979).

⁹G. Weinreich, Phys. Rev. **107**, 317 (1957).

¹⁰V. E. Henrich and G. Weinreich, Phys. Rev. **178**, 1204 (1969).

¹¹J. H. McFee, Physical Acoustics, (Academic, New York, 1966), Vol. 4, part A.

¹²N. S. Shiren, R. L. Melcher, D. K. Garrod, and T. G. Kazyaka, Phys. Rev. Lett. **31**, 819 (1973).

¹³I. A. Viktorov, Sov. Phys. Acoust. **14**, 165 (1968).

¹⁴S. Takada, K. Hoh, H. Hayakawa, and N. Mikoshiba, J. Jpn. Soc. Appl. Phys. **42**, 21 (1973).

¹⁵K. A. Ingebrigtsen, J. Appl. Phys. **41**, 454 (1970).

¹⁶J. H. Collins, K. M. Lakin, C. F. Quate, and H. J. Shaw, Appl. Phys. Lett. **13**, 314 (1968).

¹⁷V. L. Gurevich and A. L. Efros, Sov. Phys. JETP **17**, 1432 (1963).

¹⁸K. Blötekjaer, IEEE Trans. Electron Devices **ED-17**, 30 (1970).

¹⁹R. L. Gunshor, Solid State Electron. **18**, 1089 (1975).

²⁰H. Mathews, Surface Wave Filters: Design, Construction and Use (Wiley, New York 1977).

²¹A. Bers, J. H. Cafarella, and B. E. Burke, Appl. Phys. Lett. **22**, 399 (1973).

²²(a) C. Campbell, Surface Acoustic Devices and Their Signal Processing Application (Academic, San Diego, CA, 1989); (b) A. Chatterjee, P. K. Das and L. B. Milstein, IEEE Trans. Sonics and Ultrasonics **SU-32**, 745 (1985).

²³J. B. Green, and G. S. Kino, IEEE Trans. Sonics Ultrasonics **SU-32**, 734 (1985).

²⁴H. Hayakawa and G. S. Kino, Appl. Phys. Lett. **25**, 178 (1974).

²⁵S. Takada, H. Hayakawa, and N. Mikoshiba, Appl. Phys. Lett. **23**, 415 (1973).

²⁶P. S. Schenker, C. W. Lee, and R. L. Gunshor, Appl. Phys. Lett. **25**, 688 (1974).

²⁷P. Das, M. E. Motamedi, and R. T. Webster, Appl. Phys. Lett. **27**, 120 (1975).

²⁸H. Gilboa and P. Das, Solid State Electron. **22**, 55 (1978).

²⁹R. T. Webster, H. Estrade-Vazquez, P. Das, and R. Bharat, Solid State Electron. **22**, 541 (1979).

³⁰P. Das, M. K. Roy, R. T. Webster, and K. Varahramyan, Proceedings of IEEE Ultrasonic Symposium, (IEEE, New York, 1979), pp. 278–283.

³¹P. Das, R. T. Webster and B. Davari, Appl. Phys. Lett. **34**, 307 (1979).

³²H. Gilboa and P. Das, IEEE Trans. Electron. Devices, **ED-27**, 461 (1980).

³³R. Adler, D. Janes, S. Datta, and B. J. Hunsinger, in Ref. 7, p. 139–141.

³⁴F. M. Mohammed Ayub and P. Das, J. Appl. Phys. **51**, 433 (1980).

³⁵I. J. Fritz, J. Appl. Phys. **52**, 6749 (1981).

³⁶V. A. V'yun and M. D. Levin, Sov. Phys. Solid State **23**, 475 (1981).

³⁷A. I. Bul'yuk, I. M. Kotelyanskii, A. I. Krikunov, and V. N. Fedorets, Sov. Phys. Solid State **23**, 1517 (1981).

³⁸R. G. Kryshchal' and V. N. Fedorets, Sov. Phys. Acoust. **30**, 163 (1981).

³⁹V. Karahramyan and P. Das, Solid State Electron. **25**, 517 (1982).

⁴⁰B. Davari and P. Das, Proceedings of the IEEE Ultrasonic Symposium, (IEEE, New York, 1982), pp. 479–484.

⁴¹B. Davari and P. Das, Appl. Phys. Lett. **40**, 807 (1982).

⁴²B. Davari and P. Das, J. Appl. Phys. **53**, 3668 (1982).

⁴³B. Davari and P. Das, IEEE Electron Device Lett. **EDL-4**, 169 (1983).

⁴⁴P. Das, M. Tabib-Azar, B. Davari, and J. H. Everson, Proceedings of the IEEE Ultrasonic Symposium (IEEE, New York, 1983).

⁴⁵B. Davari, P. Das, and R. Bharat, J. Appl. Phys. **54**, 415 (1983).

⁴⁶B. Davari, M. Tabib-Azar, K. I. Lee, P. Das, E. Mendel, and D. A. Miller, Proceedings of International Electron Devices Meeting, (IEEE, New York, 1983), Pub. No. CH1973-7 pp. 678–681.

⁴⁷B. Davari, J. H. Everson, M. Tabib-Azar, P. Zimmermann and P. Das, Proceedings of International Electron Devices Meeting, (IEEE, New York, 1983), Pub. No. CH1973-7, pp. 678–681.

⁴⁸(a) M. Tabib-Azar, T. Liu, M. N. Abedin and P. Das, Proceedings of the IEEE Ultrasonic Symposium (IEEE, New York, 1984), pp. 926–929; (b) H. Gilboa, W. Hata, K. O'Donnell, M. Tabib-Azar and P. Das, Mater. Res. Soc. Symp. Proc. **38**, 511 (1985).

⁴⁹M. Tabib-Azar and P. Das, Proceedings of the IEEE Ultrasonic Symposium (IEEE, New York, 1985), pp. 1016–1021.

⁵⁰P. Das, M. Tabib-Azar, and J. H. Everson, Appl. Surf. Sci. **22/23**, 737 (1985).

⁵¹B. Davari and P. K. Das, IEEE Trans. Sonics Ultrasonics **SU-32**, 778 (1985).

⁵²W. C. Wang, H. Schachter, B. Elasar, S. Z. Wu and S. Onishi, IEEE Trans. Sonics Ultrasonics, **SU-32**, 645 (1985).

⁵³B. Davari, M. Tabib-Azar, T. Liu, and P. Das, Solid State Electron. **29**, 75 (1986).

⁵⁴M. Tabib-Azar, M. N. Abedin, and P. Das, Proceedings of the IEEE Ultrasonic Symposium (IEEE, New York, 1987), pp. 95–100.

⁵⁵M. Tabib-Azar and P. Das, Appl. Phys. Lett. **50**, 436 (1987).

⁵⁶F. Palma and P. Das, IEEE Ultrasonic, Ferroelectric, Frequency Control, **UFFC-34**, 376 (1987).

⁵⁷M. Tabib-Azar, Nam-Chun Park, and P. Das, Solid State Electron. **30**, 705 (1987).

- ⁵⁸M. Tabib-Azar and P. Das, *Infrared Phys.* **27**, 193 (1987).
- ⁵⁹F. Palma, L. Saccani, and P. Das, *Superlatt. Microstruct.* **3**, 181 (1987).
- ⁶⁰M. Tabib-Azar and P. Das, *Superlatt. Microstruct.* **4**, 643 (1988).
- ⁶¹M. N. Abedin, K. J. Han, and P. Das, *Proceedings of the IEEE Ultrasonic Symposium* (IEEE, New York, 1988).
- ⁶²M. Tabib-Azar and P. Das, *Appl. Phys. A* **45**, 119 (1988).
- ⁶³M. Tabib-Azar, *Solid State Electron.* **31**, 1197 (1988).
- ⁶⁴M. N. Abedin, P. Das, *Semicond. Sci. Technol.* **3**, 623 (1988).
- ⁶⁵F. Palma, P. Das, in Ref. 61, pp. 457–461.
- ⁶⁶M. N. Abedin, P. Das, A. Fathimulla, *Superlatt. Microstruct.* **4**, 333 (1988).
- ⁶⁷M. Tabib-Azar, F. Hajjar, *IEEE Trans. Electron Devices*, **ED-36**, 1189 (1989).
- ⁶⁸F. Palma, *J. Appl. Phys.* **66**, 292 (1989).
- ⁶⁹M. Tabib-Azar, *Solid State Electron.* **32**, 749 (1989).
- ⁷⁰M. N. Abedin, S. C. Tiersten, and P. Das, *Appl. Phys. Lett.* **54**, 2725 (1989).
- ⁷¹M. Tabib-Azar and M. DeGuire, *Proceedings of the IEEE Ultrasonics International Symposium* (IEEE, New York, 1989).
- ⁷²M. Tabib-Azar and F. Hajjar, in Ref. 71.
- ⁷³F. Hajjar, P. Claspay, and M. Tabib-Azar, *Solid State Electron.* **32**, 801 (1989).
- ⁷⁴F. Palma, G. de Cesare, A. Abbate, and P. Das, in Ref. 71, pp. 117–120.
- ⁷⁵F. Palma, A. Abbate and G. de Cesare, in Ref. 61, pp. 223–227.
- ⁷⁶H. Wohltjen, D. S. Ballantine, Jr., and N. L. Jarvis, in *Chemical Sensors and Microinstrumentation*, edited by R. W. Murray, R. E. Dessy, W. R. Heineman, J. Janata, and W. R. Seitz (American Chemical Society, Washington, DC, 1989) pp. 157–175.
- ⁷⁷E. T. Zellers, in Ref. 76, pp. 176–190.
- ⁷⁸A. J. Ricco *et al.*, in Ref. 76, pp. 190–207.
- ⁷⁹G. C. Frye, S. J. Martin, A. J. Ricco, and C. J. Brinker, in Ref. 76, pp. 157–175.
- ⁸⁰A. J. Ricco, S. J. Martin, and T. M. Niemczyk, 1990 IEEE Solid State Sensor and Actuator Workshop Proceedings, Hilton Head Island, S. C. June 4–7 (unpublished).